

Benchmark Project on Inelastic Deformation and Life Prediction of 2 1/4 Cr-1Mo Steel Under Multiaxial Stresses

Tatsuo Inoue
Kyoto University, Kyoto, Japan

INTRODUCTION

The Subcommittee on Inelastic Analysis and Life Prediction of High Temperature Materials (the members are listed in footnote), the Society of Material Science, Japan, has performed a cooperative project consisting of the following two tasks: (A) Review and evaluation of inelastic constitutive models relevant to the material response under plasticity-creep interaction, and (B) examination of methods of life prediction in fatigue-creep interaction.

As the first step toward the accomplishment of above two tasks, the benchmark studies had been conducted to evaluate ten kinds of constitutive models by simulating inelastic behavior in uniaxial stress state, and to examine eight types of fatigue-creep life estimation methods for 2 1/4Cr-1Mo steel at 600°C (Inoue et al, 1985; 1989a; 1989b; 1989c).

In this second phase of the project, the models and the methods are applied to multiaxial stress state of combined tension (-compression) and torsion. The present report deals with the summary of the two tasks (A) and (B). Fourteen kinds of the benchmark problems of six categories were solved by ten constitutive models to evaluate their accuracy in simulating the experimental behavior of the same material in the task (A), and life prediction under four strain wave patterns were carried out by means of seven kinds of methods in the task (B).

FUNDAMENTAL PROPERTIES OF THE MATERIAL

Normalized and tempered 2 1/4Cr-1Mo steel (ASTM SA387, Gr.22) was employed

Members of the Subcommittee on Inelastic Analysis and Life Prediction of High Temperature Materials, JSMS are T. Inoue (Kyoto Univ., Chairman); T. Igari (Mitsubishi Heavy Ind., Secretary); F. Yoshida (Hiroshima Univ., *ibid*), N. Ohno (Nagoya Univ., *ibid*), M. Kawai (Univ. Tsukuba, *ibid*), Y. Niitsu (Tokyo Inst. Tech., *ibid*), S. Imatani (Kyoto Univ., *ibid*), M. Okazaki (Nagaoka Univ. Tech., *ibid*), M. Sakane (Ritsumeikan Univ., *ibid*), S. Kishi (Toshiba, Co., *ibid*); Y. Asada (Univ. Tokyo), S. Murakami (Nagoya Univ.), S. Kubo (Osaka Univ.), K. Tanaka (Tokyo Metro. Inst. Tech.), S. Nagaki (Okayama Univ.), E. Matsumoto (Kyoto Univ.), K. Motoie (Hiroshima Denki Inst. Tech.), T. Yokobori (Tohoku Univ.), O. Watanabe (Tsukuba Univ.), H. Aono (Ishikawajima Harima Heavy Ind.), A. Suzuki (*ibid*), T. Uno (Toshiba Co.), K. Fujiyama (*ibid*), M. Matsumura (*ibid*), K. Kanazawa (National Res. Inst. Metals), H. Koto (Mitsubishi Heavy Ind.), T. Hiroe (*ibid*), K. Tokimasa (Sumitomo Metal Ind.), K. Nagato (Kawasaki Heavy Ind.), T. Horikawa (*ibid*), A. Nitta (Central Res. Inst. Elect. Power Ind.), M. Nishino (Nippon Steel Co.), T. Yokomaku (Kobe Steel Co.), Y. Wada (Power Reactor and Nucl. Fuel Dev. Co.)

throughout the project at 600°C. The chemical composition and the mechanical properties of the material at room temperature and at 600°C is presented in the first report (Inoue et al, 1989a). The material parameters in the constitutive models were identified by using the following test data under uniaxial stress:

(1) Stress-strain diagrams of five kinds of strain rates: $\dot{\epsilon} = 0.5, 10^{-1}, 10^{-2}, 10^{-3}$ and $10^{-4}\%$ /s. Since the strain rate dependence of the curve seems to be saturated approximately at the strain rate of $\dot{\epsilon} = 0.5\%$ /s, material at this strain rate is regarded as "plastic" if necessary for constitutive modeling.

(2) Data of creep strain versus time and creep rupture data under seven stress levels of $\sigma = 275, 250, 220, 180, 150, 120$ and 90 MPa.

(3) Stress-strain hysteresis loops in the strain controlled cyclic tests under three levels of strain ranges $\Delta\epsilon = 2.0, 1.2$ and 0.8% at strain rate of $\dot{\epsilon} = 0.5\%$ /s. The material cyclically hardens during the first five cycles and then cyclically softens.

(4) Fatigue-creep test data under four modes of combined of fast strain rate ($\dot{\epsilon} = 0.5\%$ /s) and slow one ($\dot{\epsilon} = 10^{-2}\%$ /s), which are used for life prediction scheme (Inoue et al, 1989b).

BENCHMARK PROBLEMS (A) FOR INELASTIC DEFORMATION AND CONSTITUTIVE MODELS

Problems

Material response for fourteen benchmark problems of six categories, as illustrated in Table 1, were simulated by the constitutive models, and compared with experimental results:

- A-I. Simple and cyclic plastic straining and creep under tension or torsion.
- A-II. Multiaxial loading under mixed mode of plasticity and creep.
- A-III. Straining in cruciform and circular shapes and creep in circular stress path.
- A-IV. Mechanical ratcheting under cyclic torsion combined with tensile stress.
- A-V. In-phase cyclic straining.
- A-VI. Out-of-phase cyclic straining.

Constitutive Models Examined

Ten types of inelastic constitutive models were evaluated in simulating the material responses in the benchmark problems. The selection of these models is more or less arbitrary, and does not reject further applications of the constitutive models proposed by many other researchers.

- (1) Superposition model, or in other words, the classical model.
- (2) Modified superposition model (Corum, Sartory, 1985).
- (3) Mroz model (Kujawski, Mroz, 1980).
- (4) Chaboche model (Chaboche, Roussellie, 1983).
- (5) Miller model (Miller, 1976).
- (6) Fraction model (Suzuki, Tsuchiya, 1986).
- (7) Ohno-Murakami model (Ohno, Kachi, 1986; Murakami, Ohno, 1982).

The brief statement of above models is presented in the reference (Inoue et al, 1989a).

(8) Endochronic model (Watanabe, Atluri, 1986): The model employed here is a modification of the original model by Valanis (Valanis, 1971) by using the isotropic hardening-type yield function and the associated flow rule.

(9) Niitsu model (Niitsu, Ikegami, 1988): This model is an extension of the fraction model, which uses a distribution function of yield stress instead of the material elements with discrete values of yield stress. The work-hardening or -softening is described by use of the hereditary integration along the plastic strain path.

(10) Imatani model (Sahashi, Imatani, Inoue, 1986): This is essentially based on the excess stress theory by Perzyna, and is extended so as to describe the plasticity creep interaction behavior by using the internal variables such as kinematic back stress and isotropic yield and drag stresses.

Table 1 Illustration of the bench mark problems (A).

Problem	Item	Diagram	
A-I Tension or torsion	I-1 Tensile or torsional plasticity	(a)	
		(b)	
	I-2 Tensile or torsional creep	(a)	
		(b)	
	I-3 Cyclic tension	(a)	
		(b)	
		(c)	
		(d)	
	A-II Plasticity creep interaction	II-1 Tensile creep Combined plasticity	
		II-2 Tensile plasticity Combined creep	
A-III Combined cyclic inelasticity	III-1 Cruciform strain path		
	III-2 Circular strain path		
	III-3 Circular stress path		
A-IV Combined ratcheting	IV-1 Fast cycling		
	IV-2 Slow cycling		

BENCHMARK PROBLEMS (B) FOR FATIGUE-CREEP LIFE AND LIFE ESTIMATION METHODS

Problems

Four kinds of fatigue-creep benchmark tests under two strain wave patterns without and with phase difference illustrated in the Problems A-V and VI of Table 1 were performed to know the number of cycles to failure. In this task (B), the names of the problems are termed as Problem B-I-1, 2 and B-II-1, 2. The thin-walled tubular specimens with outer and inner diameters of 13mm and 10mm respectively were used for experiment. In order to obtain the fundamental data, several kinds of creep-fatigue tests in uniaxial stress state were also carried out by specifying the same material, results of which have been reported in the previous paper (Inoue et al, 1989b).

Life Estimation Methods Examined

Following seven types of fatigue-creep life estimation methods are adopted in this project (B). Since the way how to apply to multiaxial stress condition is not clearly stated in some models in original papers, modifications are made by the subcommittee members, and plural members independently challenged to employ some methods.

(1) Linear Damage Rule (for brevity, LDR): Linear damage rule is a method proposed by Robinson (Robinson, 1952) and Taira (Taira, 1962), and is authorized in ASME B. & P.V. Code Case N-47. Fatigue-creep damage is divided into two parts due to fatigue D_f as a cycle fraction and creep induced damage D_c as a time fraction. Material failure is assumed to occur when a linear summation of D_f and D_c reaches a critical value D . The typical application procedure to the multiaxial stress condition is described in the Code Case N-47, but nevertheless in this project, six different ways termed as LDR-1 ~ 6 are attempted to evaluate D_f and D_c .

(2) Strain Range Partitioning Method (SRP, for brevity): Characteristics of this method (Manson, Halford, 1976) is to distinguish rate-independent plastic strain which leads to transgranular damage from rate-dependent creep strain responsible for grain boundary damage. The inelastic strain range is assumed to be composed of four specific components with the combination of fast and slow strain patterns, and these components are related to the inherent material lives which are represented by the Manson-Coffin type equations. Fatigue-creep life is now estimated by the equation called "Interaction Damage Rule".

(3) Majumdar Method: Contribution of cavity growth and crack growth to fatigue-creep damage is taken into consideration in this method (Majumdar, 1981), and the material failure is assumed to occur when either the crack length or the cavity size reaches a critical value.

(4) Ostergren Method: Ostergren emphasized the effect of a tensile peak stress during cycling as well as a cycle frequency, and proposed an equation by modifying Manson-Coffin law (Ostergren, 1976). In applying this method to multiaxial stress state, three different ways termed as Ostergren 1, 2 and 3 are tried for characterization of the peak stress and cycle frequency.

(5) Krempl Method: Evolution of fatigue damage D_f and creep damage D_c are given by the function of stress applied and inelastic strain rate, and failure is assumed to occur when total damage reaches a critical value (Sato, Krempl, 1982). In multiaxial stress state, inelastic strain rate and stress were represented by the Mises equivalent strain rate and stress in this work.

(6) Lemaitre-Plumtree-Chaboche Method: The damage rate equations for D_t of transgranular type cracking and D_i of intergranular type one are characterized based on damage mechanics concept (Lemaitre, Plumtree, 1979; Lemaitre, Chaboche, 1973).

(7) Bui-Quoc Method: The fatigue damage D_f is assumed to depend on the function of cycle fraction of fatigue life N/N_f , and the creep damage D_c , on the other hand, is represented as the function of time fraction of creep rupture time t/t_r (Bui, 1982). The creep-fatigue life is predicted when the sum of D_f and D_c reaches to unity. On applying this method to the multiaxial stress state in this work, four kinds of evaluation schemes of D_f and D_c were applied by using same schemes as LDR-1 ~ 6 in the linear damage rule, and the schemes are

named as Bui-1, 2, 3 and 4 respectively.

Details of the calculation method and the process of determination of material parameters depend on each member's interpretation of the constitutive models, and several models were examined by plural members independently. Predicted results of these models will be indicated, for example, as Supers (A), (B), (C) in the following.

RESULTS OF EVALUATION FOR INELASTIC DEFORMATION — TASK(A)

Problem A-I; Simple and Cyclic Plastic Straining and Creep under Tension or Torsion — The stress at inelastic strain of 1.0% versus strain rate reproduced from the rate dependent stress-strain curves calculated at $\dot{\epsilon} = 0.5, 10^{-1}, 10^{-2}, 10^{-3}, 10^{-4}\%/s$ are shown in the figure, as an example, together with the experimental values. In the experiments in Fig.1, the increase in flow stress decelerates as strain rate becomes higher. However, some models such as Chaboche and Imatani do not describe this tendency of deceleration with increasing flow stress, though all the models predict the increase of flow stress. Since all the constitutive models are expressed as the functions of the second invariant of deviatoric stress tensor, the predicted flow stress in tension gives the same flow stress in torsion. Actually, no apparent difference in flow stress is found in the experiments between tension and torsion.

Figure 2 shows the relation between creep strain at 10h and applied stress level reproduced from the calculated creep curves, together with the experimental results in tension and torsion. The calculated results by the simple and modified superposition models and the Mroz model agree very well with the experimental results, since these models use the creep data themselves in determining the material parameters of their creep equations. The endochronic mode, the Chaboche model(B) and the Ohno-Murakami model(B) can also simulate the actual creep behavior fairly well. In some of the unified constitutive models, such as the Fraction model and the Ohno-Murakami model, the material parameters are determined on the basis of the tension test data rather than the creep data, hence an accurate prediction for creep is not always assured by these models. In the other group of the unified constitutive models, e.g. the Chaboche and the endchronic models, the creep data are mainly used, together with a part of ten-

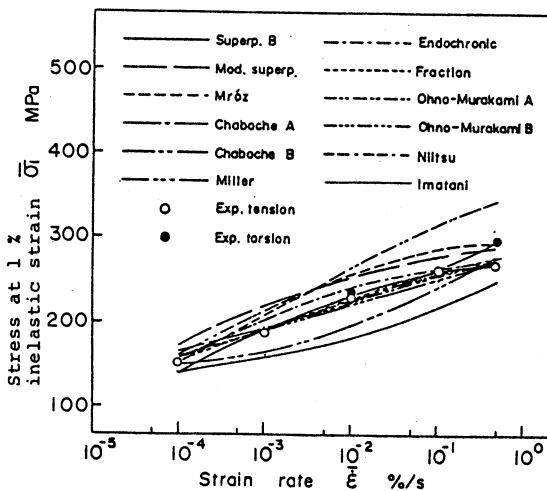


Fig.1 Strain rate dependence of flow stress $\bar{\sigma}_1$ at 1% proof strain — Problem A-I-1 —.

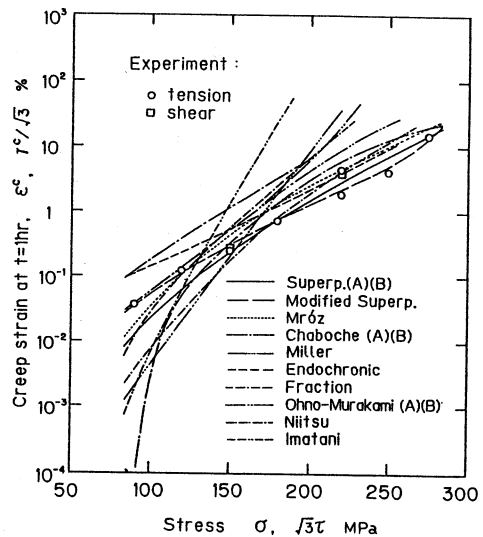


Fig.2 Creep strain at 10h exposed to given stress — Problem A-I-2 —.

sion test data for the determination of the parameters. The predictions of rate-dependent behavior of flow stress in the tension tests by these models are in worse agreements with the experimental results.

Problem A-II; Multiaxial Loading under Mixed Mode of Plasticity and Creep — Figure 3 illustrates the subsequent stress loci at effective plastic strain of 0.1% after the tensile creep in Problem II-1, together with the experimental result. The predictions by most of the unified models give the anisotropic hardening, except for the results by the Miller and the Niitsu models. Especially for the subsequent compression test ($\theta = 180^\circ$), some unified models such as the endochronic model, the Ohno-Murakami model(A) and (B) give the remarkable Bauschinger effect. Let us discuss the effect of plastic straining on the subsequent creep under multiaxial stress state. The subsequent creep strain loci at 1h after 2.0% tensile plastic prestrain in Problem II-2 is shown in Fig.4 together with the experimental results. Few constitutive models can describe accurately the anisotropic hardening characteristics that the material does not harden in the direction of plastic prestraining by softens considerably in the opposite direction, though some models can simulate the hardening or softening behavior for one of the directions.

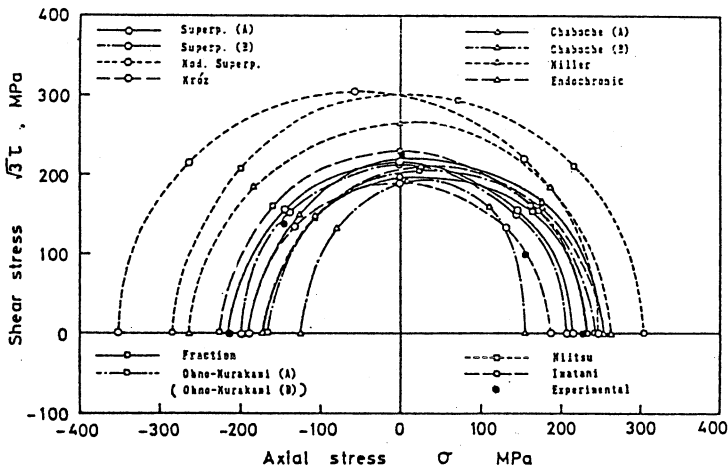


Fig.3 The subsequent stress loci at effective plastic strain of 0.1% after tensile creep — Problem A-II-1 —.

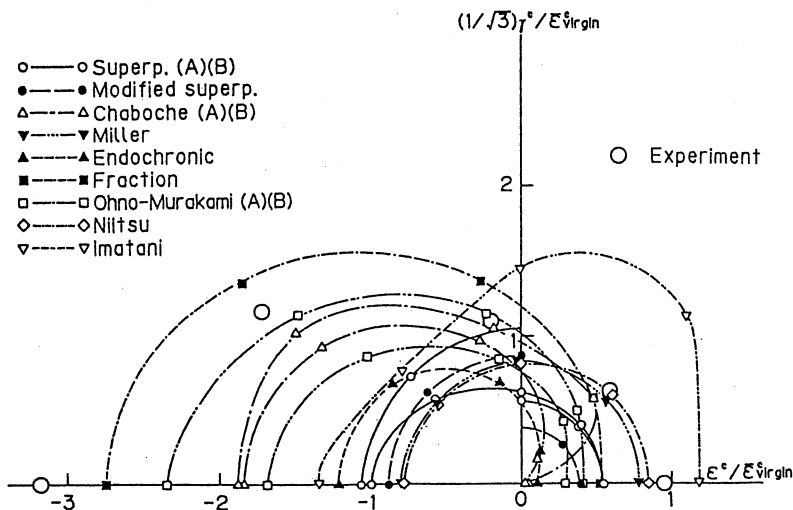


Fig.4 The subsequent creep strain loci at 1h after plastic prestrain of 2.0% — Problem A-II-2 —.

Problem A-III; Straining in Cruciform and Circular Shapes and Creep in Circular Stress Path — Figure 5(b) represents the experimental stress response for cruciform strain path illustrated in Fig.(a). Figure 5(c) depicts the calculated stress range and the ratio of the stress range $\lambda = \Delta\sigma_A / \Delta\sigma_B$ being compared with the experimental results, where the stress range $\Delta\sigma_A$ and $\Delta\sigma_B$ are defined as the axial peak-to-peak stress from the point ① to ⑤ and the stress range from ② to ⑥ in Fig.5(b), respectively. The ratio of the stress range $\Delta\sigma_A$ represents the Bauschinger effect in the cruciform straining, i.e., the smaller value of λ indicates the stronger Bauschinger effect, and no Bauschinger effect appears when $\lambda=1$. The peak-to-peak stress value λ is about 10% higher than that of uniaxial cyclic straining. Most of the models can hardly express this additional hardening induced by the cruciform cyclic straining. The predicted values of λ by the Mroz, the Chaboche(B), the endochronic and the Ohno-Murakami(A) and (B) models give the good agreement with the experimental value. It means that these models simulate the actual behavior of the Bauschinger effect in the cruciform straining.

The stress path in the experiment of the circular straining (Problem III-2) is represented in Fig.6(a). Each shape of the stress paths is a circle in the 1st strain cycle to the 10th (the 1st block), the 11th to the 20th (the 2nd block) and the 21st to the 30th (the 3rd block). Figure 6(b) demonstrates the comparison of the stress amplitude between the calculated value and the experimental result, which is defined as the radius of the stress path, at the 5th, the 15th and the 25th cycles as the representative values in the 1st, the 2nd and the 3rd blocks of the circular straining. Most of the models describe the experimental tendency of stress amplitude change that the stress amplitude in the 2nd block becomes the smallest because of the lowest strain rate, and the amplitude in the 1st block is larger than that in the 3rd block owing to cyclic softening. Especially the Chaboche model(A) and the Ohno-Murakami model(B) can

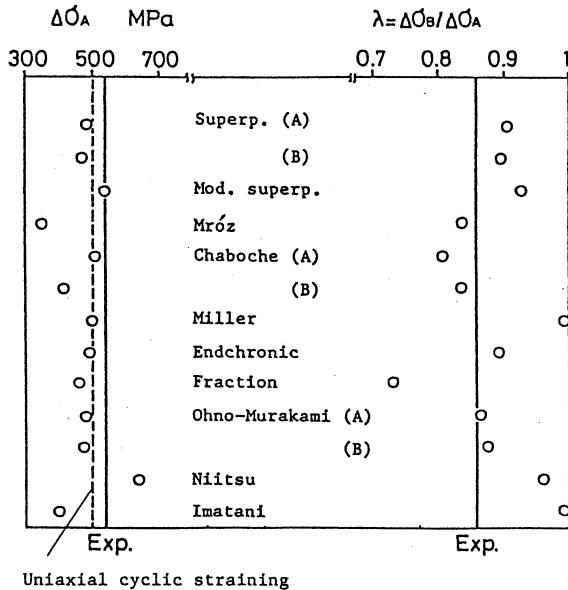
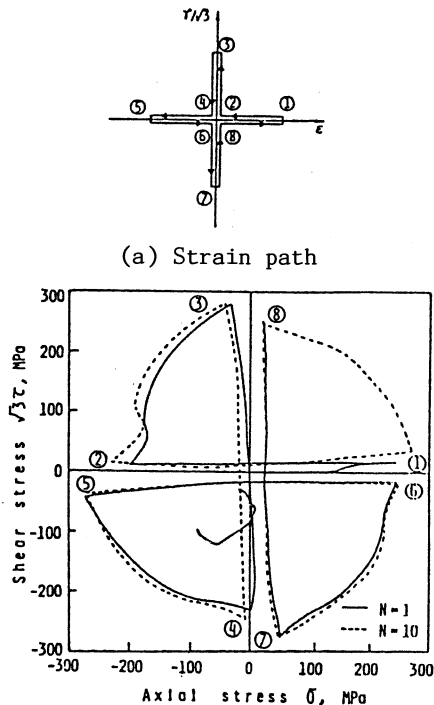
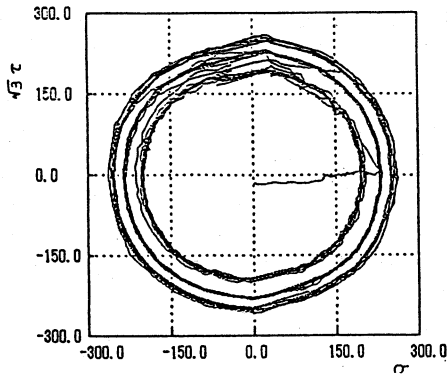
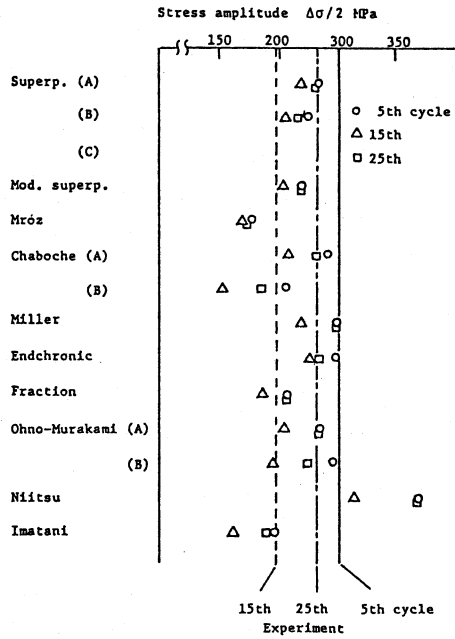


Fig.5 Response at the 1st and 10th cycles in the cruciform strain — Problem A-III-1 —



(a) Experimental stress circle



(b) Calculated stress amplitude

Fig.6 Stress response for circular straining — Problem A-II-2 —.

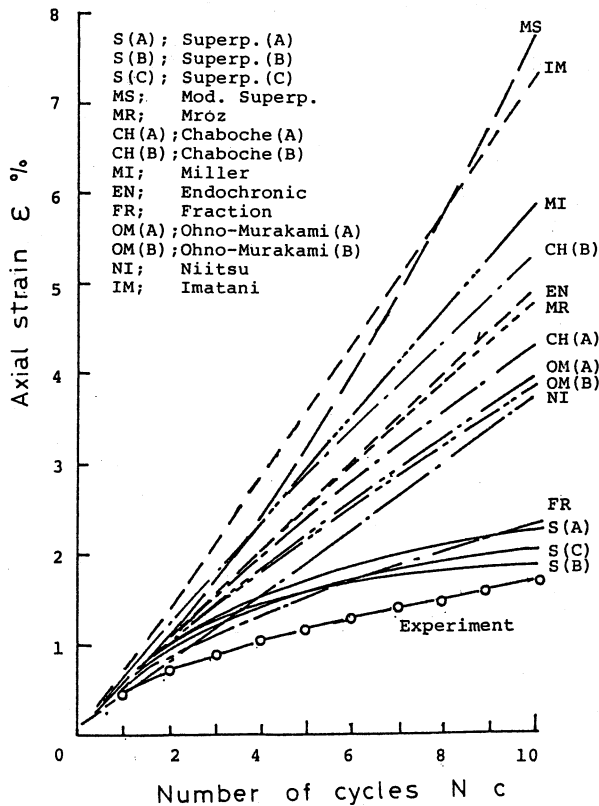


Fig.7 Axial strain accumulations in multiaxial mechanical ratcheting at fast cycling of $\dot{\gamma}/\sqrt{3}=0.1\%/s$ — Problem A-IV-1 —.

predict the behavior quantitatively, whereas some models, e.g. the Mroz, the Chaboche (B) and the Imatani models, underestimate the stress amplitude, and the Niitsu model overestimates it.

Problem A-IV; Mechanical Ratcheting under Cyclic Torsion Combined with Tensile Stress — Accumulated axial strain due to the multiaxial ratcheting of Problem IV-1 is presented in Fig.7. The rate of strain accumulation is high in the first few strain cycles, and it gradually decelerate with increasing number of cycles. The superposition models(A), (B), (C) and the fraction model can simulate rather well the experimental result, although all the predictions by the constitutive models overestimate the strain accumulation. The strain accumulation in the slow cycling of Problem IV-2 is about 1.5 times larger than in the fast cycling of Problem IV-3. All the models can describe this experimental tendency.

The stress-strain responses in the in-phase and out-of-phase cyclic straining (Problem VI and V) will be stated in next section, since the problems are closely related to life prediction under fatigue-creep regime.

RESULTS OF ESTIMATION OF FATIGUE-CREEP LIFE — TASK(B)

Summary of the experimental life is given in Fig.8. The vertical axis in the figure indicates the Mises equivalent strain range defined in ASME B. & P.V. Code Case N-47. The experimental data in uniaxial stress state are also plotted in the figure for comparison. Little difference is found between uniaxial and multiaxial fatigue life under the in-phase condition of fast-fast and slow-slow cycling, while under out-of-phase pattern of slow-slow cycling the multiaxial fatigue life is notably shorter than the corresponding uniaxial fatigue life.

Results based on Experimental Stress-strain Behavior

The predicted fatigue lives by means of prediction methods mentioned previously are summarized in Fig.9. It can be seen that all methods give the predicted life within a factor of two. As for the predicted results under out-of-phase pattern, following three characteristics can be pointed out: Firstly, the effect of the difference of the definition of equivalent stress on prediction life can be seen, e.g. in the linear damage rule, between LDR-1 and 2, LDR-3 and 4, and LDR-5 and 6. It follows that the prediction method in term of the Mises

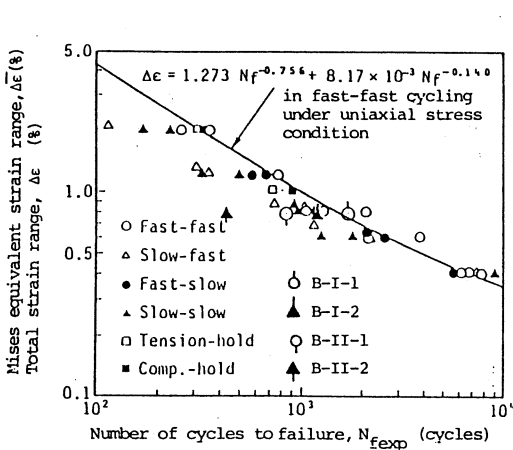


Fig.8 Summary of experimental results of fatigue-creep lives — Problem B —.

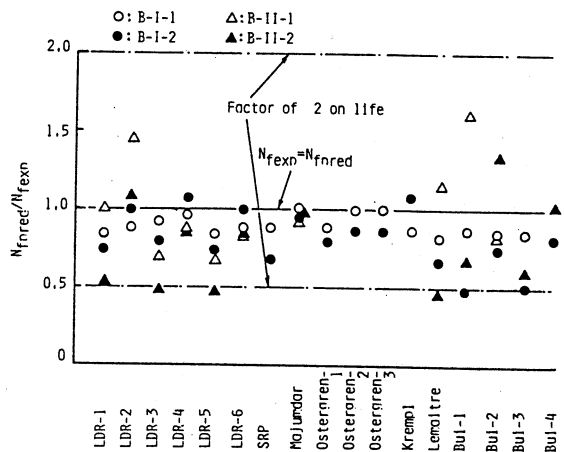


Fig.9 Summary of predicted lives by life estimation methods — Problem B —.

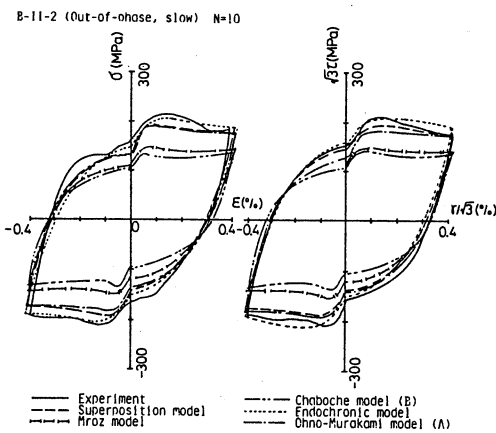
equivalent stress does not give better prediction than by more sophisticated definition of equivalent stress like Huddleston's (Huddleston, 1985). Similar tendency is also found in Ostergren and Bui-Quoc methods. Therefore, it can not be concluded that the Mises equivalent stress is successful parameter enough to describe the multiaxial creep-fatigue life, especially in out-of-phase pattern.

The prediction methods in which the special attention on the failure under multiaxial loading condition is paid to give most preferable prediction. For example, Majumdar method with the parameters representing the effect of multi-axiality estimates the good result. Similar tendency can be also found in Ostergren method. Therefore, we may say that it is inevitable for multiaxial creep-fatigue life prediction to precisely understand the failure characteristics as well as to establish the failure criterion.

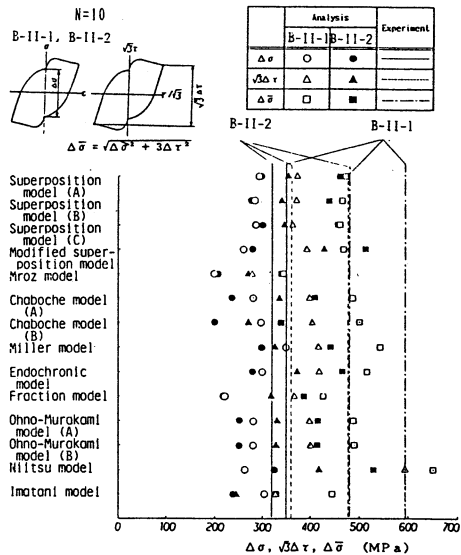
Results based on Analytical Stress-Strain Behavior

The life prediction based on the analytical stress-strain behavior is carried out by employing three prediction methods of linear damage rule (LDR), strain range partitioning method (SRP) and Majumdar method. In LDR and Majumdar methods, ten kinds of inelastic constitutive models are employed to evaluate stress-strain response. While in SRP, five kinds of constitutive models are used.

The hysteresis loops at the 10th cycle calculated by some constitutive models under out-of-phase condition in slow strain cycling are shown in Fig.10(a). All constitutive models give well the characteristic hysteresis loop under out-of-phase condition. The calculated result of stress ranges $\Delta\sigma$, $\sqrt{3}\Delta\tau$ and $\Delta\bar{\sigma} [=(\sigma^2 + 3\tau^2)^{1/2}]$ at the 10th cycle under out-of-phase condition by each constitutive model are shown in Fig.10(b). This figure indicates that the analytical values obtained by all constitutive models comparatively agreed with the experimental results. Similar characteristics was also found under in-phase condition.



(a) Stress-strain hysteresis loops



(b) Stress ranges

Fig.10 Stress response for out-of-phase strain pattern — Problem B-II —.

Some examples of the predicted lives are given in Figs.11(a),(b) and (c) by LDR, SRP and Majumdar methods. Although the strict discussion can not be made on each predicted result because of limited number of experimental results, the general tendency of life prediction based on the analytical stress-strain behavior are summarized as follows: While the difference between the predicted life and experimental one is generally larger than that based on the experimental one, the amount of scatters is not serious in the practical usage. This result suggests the possibility to predict the multiaxial failure life under fatigue-creep regime by combining the inelastic constitutive equations and the simple data of uniaxial fatigue-creep tests.

Though the difference of the predicted lives by the constitutive models used is not notable, the accuracy of equivalent stress range directly affects the predicted life. This would be related to the fact that all experiments were carried out under strain-controlled condition. Regarding to the stress and strain relation used for the prediction, similar characteristics of the depen-

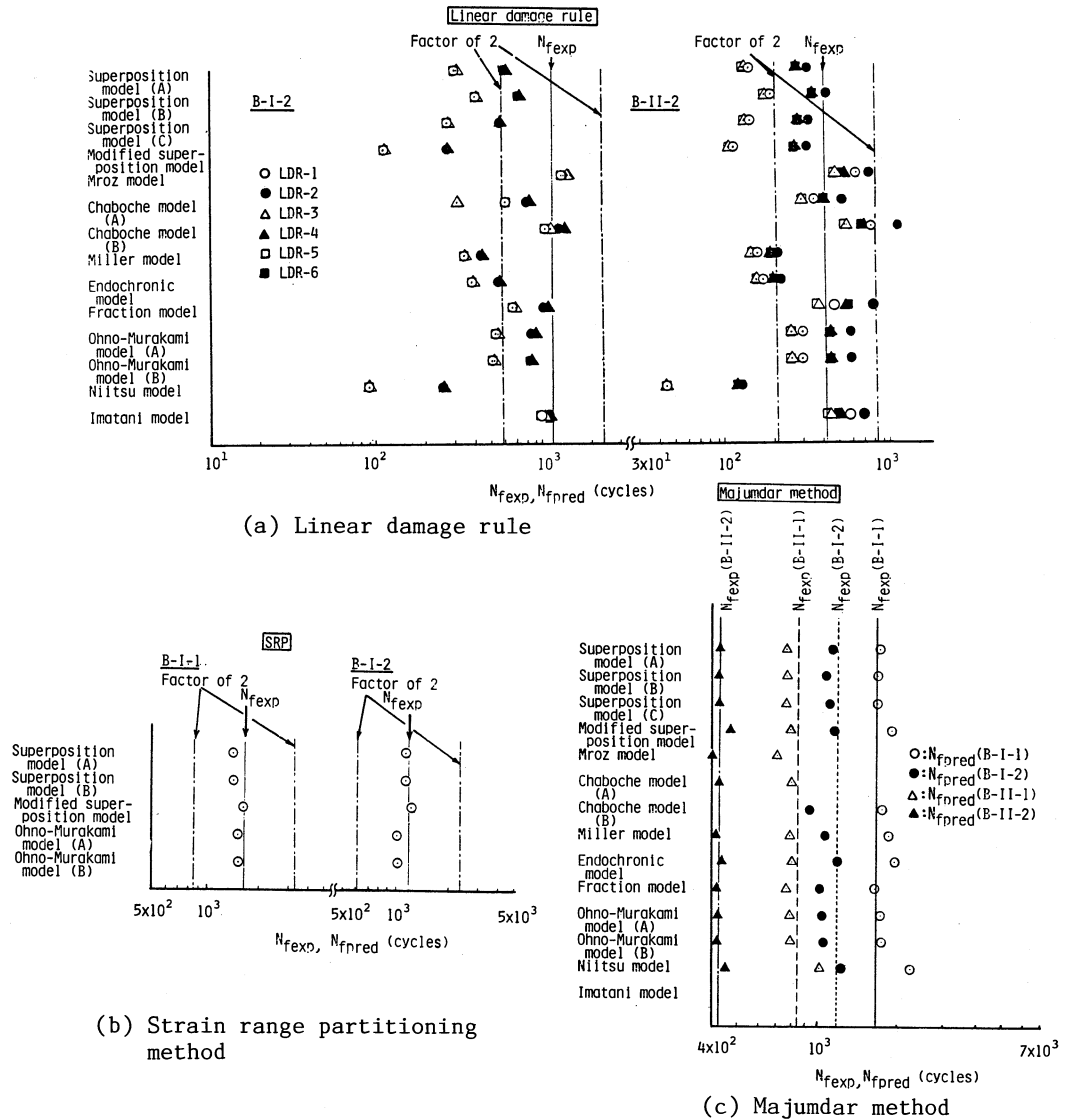


Fig.11 Predicted fatigue-creep lives based on analytical stress-strain relations — Problem B —.

dence of stress and strain on estimated life as described in the previous section, are also found in this scheme.

CONCLUDING REMARKS

To evaluate the validity and applicability of existing inelastic constitutive models under plasticity-creep interaction condition and life prediction methods in fatigue-creep regime, cooperative benchmark projects were carried out, and the results are summarized in this report. Here, attention is focused on the material behavior under multiaxial stress state.

Since the models and the methods are now in progress, we cannot reach the final goal on what kinds of models and methods are most suitable for practical usage. However, the results show that some kinds of models or methods predict the experimental data fairly well, and that others cannot. The subcommittee is now the third phase of project on the applicability of thus obtained results to finite element implementation, the results of which are expected to appear in a couple of years.

ACKNOWLEDGMENT

The subcommittee wishes to express her gratitude to the head Committee on High Temperature Strength, JSMS, for supporting the project, and acknowledgment is also due to the Ministry of Education and Culture for providing Grant-in-Aid for Co-operative Research A (No. 61302036)

REFERENCES

- ASME, B. & P.V. Code Case, N-47.
Bui-Quoc, T. and Biron, A., (1982) Nucl. Eng. Design, Vol.70, pp.89-102.
Chaboche, J.L. and Rousselle, G., (1983) Trans. ASME PVT, Vol.105, pp.153-164.
Corum, J.C. and Sartory, W.K., (1985) Preprint of the 5th Int. Semi. Inelastic Analysis and Life Prediction in High Temperature Environment, pp.419-434.
Huddleston, R.C., (1985) Trans. ASME PVT, Vol.107, pp.421-429.
Inoue, T., Igari, T., Yoshida, F., Suzuki, A. and Murakami, S., (1985) Nucl. Eng. Design, Vol.90, pp.287-297.
Inoue, T., Ohno, N., Suzuki, A. and Igari, T., (to be published, 1989) Nucl. Eng. Design.
Inoue, T., Igari, T., Okazaki, M., Sakane, M. and Tokimasa, K., (to be published, 1989) Nucl. Eng. Design.
Inoue, T., Okazaki, M., Igari, T., Sakane, M. and Kishi, S., (to be submitted, 1989) ASME 1989 PVP Conference.
Kujawski, D. and Mroz, Z., (1980) Acta Mech., Vol.36, pp.213-230.
Lemaitre, J. and Chaboche, J.L., (1973) J. Mecanique Applique, Vol.2, pp.3-10.
Lemaitre, J. and Plumtree, A., (1979) Trans. ASME EMT, Vol.101, pp.284-292.
Majumdar, S., (1981) Nucl. Eng. Design, Vol.63, pp.121-130.
Manson, S.S. and Halford, G.R., (1976) ASME MPC Symposium, pp.229-240.
Miller, A., (1976) Trans. ASME EMT, Vol.98, pp.97-113.
Murakami, S. and Ohno, N., (1982) Int. J. Solids & Struct., Vol.18, pp.597-609.
Niitsu, Y. and Ikegami, K., (1983) Trans. JSME (A), Vol.54-50, pp.1035-1043.
Ohno, N. and Kachi, Y., (1986) Trans. ASME AM, Vol.53, pp.395-403.
Ostergren, W.J., (1976) J. Test. & Eval., Vol.4, pp.327-339.
Robinson, E.L., (1952) Trans. ASME, Vol.74, pp.771-781.
Sahashi, T., Imatani, S. and Inoue, T., (1986) Trans. JSME (A), Vol.52-476, pp.1126-1133.
Satoh, M. and Krempl, E., (1982) Trans. ASME PVT, Vol.60, pp.71-79.
Suzuki, A. and Tsuchiya, A., (1986) Proc. Int. Conf. on Creep, Tokyo, Japan, pp.471-476.
Taira, S., (1962) Creep in Structures, N.J. Hoff ed., pp.96-124.
Valanis, K.C., (1972) Arch. Mech., Vol.23, pp.517-551.
Watanabe, O. and Atluri, S.N., (1986) Int. J. Plast., Vol.2-2, pp.107-134.